Received October 2, 2019, accepted October 15, 2019, date of publication October 29, 2019, date of current version November 14, 2019.

Digital Object Identifier 10.1109/ACCESS.2019.2950265

Adaptively Hybrid 3rd Simplified Spherical Harmonics With Diffusion Equation-Based Multispectral Cerenkov Luminescence Tomography

LIN WANG[1], HONGHAO CAO[2], XIN CAO[1], SHENGHAN REN[2], KE LI[3], YONGHUA ZHAN[2], XUELI CHEN[2], AND XIAOWEI HE[1]

[1]School of Information Sciences and Technology, Northwest University, Xi'an 710127, China
[2]Engineering Research Center of Molecular and Neuro Imaging, School of Life Science and Technology, Ministry of Education, Xidian University, Xi'an 710071, China
[3]Shaanxi Laboratory of Ischemic Cardiovascular Disease, Institute of Basic and Translational Medicine, Xi'an Medical University, Xi'an 710032, China

Corresponding authors: Xueli Chen (xlchen@xidian.edu.cn) and Xiaowei He (hexw@nwe.edu.cn)

This work was supported in part by the National Key Research and Development Program of China under Grant 2018YFC0910602, in part by the National Natural Science Foundation of China under Grant 81627807, Grant 81571725, and Grant 61701403, in part by the Fok Ying–Tong Education Foundation of China under Grant 161104, in part by the Research Fund for Young Star of Science and Technology in Shaanxi Province under Grant 2018KJXX-018, in part by the China Post-Doctoral Science Foundation under Grant 2018M643719, and in part by the Young Talent Support Program of the Shaanxi Association for Science and Technology under Grant 20190107.

ABSTRACT Cerenkov luminescence tomography (CLT) can reproduce the location of the tumor inside the body and the physiological processes that are related to its biological behavior, it has thus attracted more attention in the field of imaging technology. The inadequacy of signals that are measured on the body surface might cause ill-posed problems during image reconstruction, thus affecting the quantitative accuracy of CLT. This can be improved using a multispectral strategy by providing more measurements. However, current reconstruction algorithms for multispectral CLT are based on the light transport model that uses a single equation (a diffusion equation or a 3rd simplified spherical harmonics equation) for each spectrum, which cannot guarantee the accuracy and efficiency of the reconstruction. In order to make full use of the broad-spectrum characteristics of Cerenkov luminescence and ensure an accurate and efficient reconstruction, in this work we apply an adaptively hybrid model to the multispectral CLT, that can automatically select the light transport equation. Here, the hybrid model was not only applied to different spectra, but also to different tissues at a certain spectrum. The selection of the light transport equation was accomplished by automatically comparing the index with a predefined threshold. Our proposed method was evaluated with numerical simulations and mouse-based experiments and the results showed the feasibility and effectiveness of the adaptively hybrid model based multispectral CLT.

INDEX TERMS Cerenkov luminescence tomography, multispectral, hybrid method.

I. INTRODUCTION

Cerenkov luminescence imaging (CLI) is a promising small animal imaging technology that is based on the Cerenkov luminescence (CL) emission effect [1]–[6] that could be explained as follows: When the velocity of the charged particles in the medium is faster than the velocity of light, the near infrared and visible light would be emitted, and this phenomenon is called CL emission effect [7]. Based on such effect, one can then use an optical method to collect the luminescent signals upon radionuclide decay so that a seamless fusion bridge can be established between optical imaging and nuclear imaging. The problem of limited probes for translating optical imaging to clinics can be solved with the use of the widely clinically-used radionuclide probes. Since Robertson used a CCD camera to collect the CL from a small animal for the first time in 2009, CLI has been rapidly developed and widely used in the biomedical field [2], [8]–[11]. Examples include monitoring the expression of thyroid cancer cells [12], intraoperative assessment of tumor resection

The associate editor coordinating the review of this manuscript and approving it for publication was Kumaradevan Punithakumar.

margin [13], [14], assessing lymphoma treatment [15] as well as some preliminary clinical studies [16]–[19]. Using a single radionuclide probe to realize a dual-modality of optical and nuclear imaging, CLI has paved the way for a new direction in the translation of molecular imaging technology. However, since CLI is a two-dimensional (2D) planar imaging method, it can neither accurately quantify and analyze the target molecule nor provide its three-dimensional (3D) spatial information. This problem can be solved using its 3D derivative termed the Cerenkov luminescence tomography (CLT).

CLT can reconstruct the distribution of internal radionuclides using the surface measurements [20]–[24]. The concept of CLT was first proposed by Li *et al.* to reconstruct the 3D distribution ^{18}FDG in a homogeneous mouse model [20]. However, due to the fact that the inverse reconstruction is an ill-posed problem, the quality of the results needs further improvement. Based on the regularization strategy, there are two popular ways to reduce the ill-posedness and improve the quality of the reconstruction results. First, by incorporating the source permissible region which will greatly reduce the dimension of the variables to be reconstructed [25], [26], thus weakening the ill-posedness to a certain extent. The drawbacks of this method are the very limited improvement of ill-posedness and that the selection of the source permissible region is a very difficult problem, which is greatly influenced by the subjective consciousness of the operators [27], [28]. Second, we can increase the dimensionality of the measured data through multispectral measurements [29]–[31]. Multispectral strategy is suitable for CLT because the CL emission has broad spectrum characteristics [2], with a spectrum in the range of 400 to 900 nm. This method (multispectral CLT, mCLT) was first applied by Spinelli et al. and the results showed an improved reconstruction quality [29]. Following this, Guo et al. proposed a modified weight multispectral CLT to further improve the accuracy and stability of the reconstruction [30]. However, both used diffusion equation (DE) as the forward model to characterize the CL light propagation. Since DE is not accurate enough for the low scattering tissue, due to the highly-diffuse hypothesis, it is thus not suitable for mCLT. To overcome the accuracy problem, Liu et al. developed a multispectral hybrid CLT, in which the different orders of the spherical harmonics (SP_N) equation were used to describe the propagation of CL light at different wavelengths [31]. However, this method has two limitations. On the one hand, the use of the SP_N equation will increase the reconstruction time cost, especially when the order N is high, or the multispectral imaging is performed. On the other hand, the combination of high and low orders of the SP_N equation only occurs in different spectral bands. Therefore, it is hard to determine in which spectral band can the lower or higher order equation be used. An additional problem is that different tissues may exhibit different scattering characteristics within the same spectral band. In this case, the method proposed in Liu's work may not be the best solution for mCLT; using the fixed equation at a spectral band will hinder the integration of accuracy and efficiency.

In this work, we propose a reconstruction framework for mCLT based on adaptively hybrid 3rd simplified spherical harmonics with diffusion (AHSD) equation. In this framework, the AHSD equation was applied to describe CL propagation in the tissues, which fully considered and utilized the wide spectrum characteristics of the CL signal. Unlike other existing multispectral methods, the hybrid model used in this framework was not only applied to different spectra, but also to different tissues at a certain spectrum. The selection of the light transport equation was achieved by automatically comparing the index with a predefined threshold. This method outperforms the existing methods in terms of applicability, maneuverability and the combination of accuracy and efficiency. The adaptively hybrid model based mCLT was then evaluated with numerical simulations and mouse-based experiments to show the feasibility and effectiveness of the proposed method.

II. METHODS

Biological tissues inside the living body can be divided into several components based on the anatomical structure, including the heart, liver, lungs, stomach, kidneys and others. The optical properties of these components are different even at the same wavelength. Therefore, using a single equation or a hybrid equation integrated by wavelength to describe the light propagation in these tissues would not the best option. In our previous studies [32], [33], a fully hybrid model that integrated SP_N with DE was developed to accurately and efficiently achieve this task. Since the 3rd order SP_N has the sufficient accuracy and promising efficiency, the SP_3 equation was used to construct the adaptively hybrid 3rd simplified spherical harmonics with diffusion (AHSD) equation. The AHSD equation used in this work can be summarized as follows [32], [33]:

$$\begin{aligned} -\nabla \cdot C_{k,\nabla\Phi_1}(\vec{r})\nabla\Phi_1(\vec{r}) - \nabla \cdot C_{k,\nabla\Phi_2}(\vec{r})\nabla\Phi_2(\vec{r})\vec{r} \in \Omega \\ + C_{k,\Phi_1}(\vec{r})\Phi_1(\vec{r}) + C_{k,\Phi 2}(\vec{r})\Phi_2(\vec{r}) = C_{k,s(\vec{r})}S(\vec{r}) \end{aligned} \quad (1)$$

where $\Phi_k(\vec{r})$ (k = 1, 2) represent the luminous flux components at node, $S(\vec{r})$ represents the density distribution of the radioactive tracer, Ω denotes the domain of the scattering tissues and $C_{k,\nabla\Phi_1}(\vec{r})$, $C_{k,\nabla\Phi_2}(\vec{r})$, $C_{k,\Phi_1}(\vec{r})$, $C_{k,\Phi 2}(\vec{r})$ and $C_{k,s(\vec{r})}S(\vec{r})$ are the tissues' optical properties and boundary related parameters [32]. The adaptively hybrid process was achieved by automatically comparing the index with a predefined threshold. The index was defined as the ratio of the reduced scattering coefficient μ_s' to the absorption coefficient μ_a. The threshold was retrieved from existing literature and set to 10 [34]–[38]. If the index is larger than the threshold, the tissue would be classified as a high scattering region and the DE equation would be used to used to describe the CL light propagation in it; otherwise, the tissue would be sorted as a low scattering region and the SP3 would be used. This classification process can be programmed and automatically completed, and the selection of different equations is not determined by wavelength, thus avoiding the problems in existing methods.

The luminous flux density at the tissue-medium interface can be calculated as [32]:

$$J(\vec{r}) = \beta_1(\vec{r})\Phi_1(\vec{r}) + \beta_2(\vec{r})\Phi_2(\vec{r})\vec{r} \in B \tag{2}$$

where $\beta_k(\vec{r})$ (k = 1, 2) are boundary related constants of a point $\vec{r}$ at the boundary B and can be referenced from [32], [34] and $J(\vec{r})$ is the exiting partial luminescent flux density.

Combining Eq. (1) and Eq. (2), and using the finite element discretization, we can establish the relationship between the expected distribution of the radioactive tracer and the exiting partial luminescent flux density at the boundary. Eq. (1) can then be transferred as follows:

$$J = AS \tag{3}$$

where A denotes the system matrix obtained by the AHSD equation with the detailed form listed in [32] and J is the exiting partial luminescent flux density measured on the surface and S is the source distribution of the radioactive tracer.

As mentioned earlier, the CL light has wide spectral properties in the range of 400 to 900 nm; thus, the multispectral strategy is the most suitable for CLT. When we construct the system matrix at each wavelength based on the AHSD equation and incorporate the multispectral measurements, we obtain the following new matrix equation:

$$\begin{bmatrix} A(\lambda_1) \\ A(\lambda_2) \\ \vdots \\ A(\lambda_k) \end{bmatrix} S = \begin{bmatrix} J(\lambda_1) \\ J(\lambda_2) \\ \vdots \\ J(\lambda_k) \end{bmatrix} \tag{4}$$

where $A(\lambda_i)$ (i = 1,2,...,k) stands for the system matrix obtained using the AHSD equation at the wavelength of λ_i and $J(\lambda_i)$ (i = 1,2,...,k) represents the surface measurements at the wavelength of λ_i. Equation (4) can be further summarized as:

$$\mathrm{AS} = \mathrm{J} \tag{5}$$

where A and J have the following expressions:

$$\mathrm{A} = \begin{bmatrix} A(\lambda_1) \\ A(\lambda_2) \\ \vdots \\ A(\lambda_k) \end{bmatrix} \quad \text{and } \mathrm{J} = \begin{bmatrix} J(\lambda_1) \\ J(\lambda_2) \\ \vdots \\ J(\lambda_k) \end{bmatrix} \tag{6}$$

Equation (5) represents the forward model for mCLT based on the AHSD equation. The inverse reconstruction of mCLT based on AHSD can approximately be regarded as a basis pursuit problem. Taking the sparse distribution of the radioactive tracer into account, finding the solution to Eq. (5) can thus be converted into solving the following l_1-norm-based regularization problem:

$$\mathrm{S} = \arg\min \frac{1}{2} \|\mathrm{AS} - \mathrm{J}\|_2^2 + \mu \, |\mathrm{S}|_1 \tag{7}$$

where μ is the regularization parameter that was manually determined by experience throughout the following experiments. In a more advanced version, this regularization parameter can also be selected by being iteratively updated [39]. Usually, l_0-norm is used to describe the sparse property, which counts the number of non-zero elements in a given vector. However, this is a difficult combinational problem and has exponential complexity. Thus, l_1-norm regularization, that is easier to solve, is usually used to find the solution satisfying sparsity. Equation (7) is the most basic and commonly used objective function in optical tomography based on sparse reconstruction and was solved by the primal-dual interior-point algorithm in this work [40].

III. EXPERIMENTS AND RESULTS

A. DIGITAL MOUSE BASED SIMULATION

In this section, numerical simulation and *in vivo* experiments were conducted to evaluate the feasibility and effectiveness of the proposed AHSD equation based mCLT method. To make the calculations more convenient and considering that this work mainly aims to verify the feasibility and applicability of the proposed method, three wavelengths were used for the multispectral reconstruction. To evaluate the reconstruction results, two popular indicators were used: the distance between the reconstructed central position and the actual center of the radioactive tracer (Dis_Err, in units of mm) and the reconstruction time (Time, in units of second) that records the construction time of the system matrix. Furthermore, two other statistical measurements: structural similarity (SSIM) and root mean square error (RMSE), were used to evaluate the shape and quantitative distribution recovering abilities of the reconstruction methods. The detailed physical explanations and mathematical formulas of SSIM and RMSE can be retrieved from the references [41], [42]. To validate the accuracy and evaluate the superiority of the proposed method, other methods were selected as references, including the SP_3 and DE based methods, a hybrid based model constructed using SP_3 at the lower wavelength and DE at the other two higher wavelengths (abbreviated as the HSDD) and another hybrid based model built using SP_3 at the two lower wavelengths and DE at the other highest wavelength (abbreviated as the HSSD).

In this simulation, a digital mouse was used to evaluate the performance of the proposed AHSD based reconstruction method. To perform multispectral reconstruction, three wavelengths: 550 nm, 600 nm and 650 nm were utilized. The selected tissues and their relevant optical properties at these selected wavelengths are listed in Table 1. The optical properties were calculated using the formula summarized in [43]. In order to simulate the radioactive tracer, a light source was implanted into the adipose at the coordinate position of (20,11,20) mm with the radius of the light source being 1 mm, the initial power equal to 1 nW and a half-life decay of 110 minutes. The selected organs of the digital mouse included the heart, lung, stomach, liver, kidney and adipose, as shown in Fig. 1(a), where the coordinate system of the reference system is also presented. The digital mouse was discretized into a fine mesh of 93,112 tetrahedrons and 16,765 nodes, that was used as the forward mesh to calculate the surface measurements. With regard to accuracy and

TABLE 1. Optical parameters of different tissues in the digital mouse. In units of mm^{-1}.

Tissues	650 nm		600 nm		550 nm	
	μ_a	μ_s'	μ_a	μ_s'	μ_a	μ_s'
Adipose	0.0050	1.2273	0.0199	1.2805	0.0889	1.3409
Stomach	0.0149	1.4798	0.0603	1.5993	0.2694	1.7401
Lung	0.2630	2.2091	1.0410	2.3048	4.1657	2.4136
Liver	0.1021	2.4144	0.4643	3.5857	1.9245	4.7486
Heart	0.0786	1.0066	0.3163	1.1286	1.3608	1.2782
Kidney	0.0881	2.3585	0.3543	2.6615	1.5240	3.0352

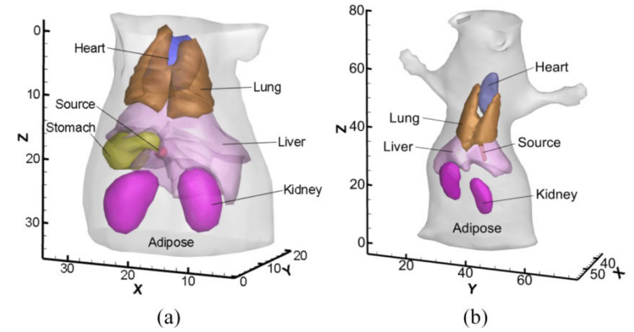

FIGURE 1. Physical models used in the simulation and in vivo experiment. (a) Digital mouse used in the numerical simulation; (b) Real mouse used in the in vivo experiment.

efficiency, these surface measurements were calculated using the SP_3 equation. For the inverse reconstruction, the digital mouse was discretized into a coarse mesh of 15,141 tetrahedrons and 3,050 nodes. After that, the localization and distribution of the radioactive tracer were reconstructed using the AHSD based method and other reference methods.

The reconstruction results obtained using the proposed and reference methods are shown in Fig. 2. In Fig. 2(a)-2(e) we show the 3D views of the reconstructed results of the AHSD, SP_3, DE, HSSD and HSDD based reconstruction methods; their sectional images are shown in Fig. 2(f)-2(j), respectively. The solid sphere in the 3D views and the black circle in the sectional images labeled the actual position of the radioactive tracer, while the colored tetrahedrons are the reconstructed sources. Our experiment shows that the reconstructed images have almost the same quality using the AHSD and SP_3 based reconstruction methods that is better than the reconstruction quality of the DE, HSDD and HSSD based methods, with the image reconstructed by the DE based method having the worst quality. Two other interesting phenomena can be found in the sectional images. First, the AHSD based method provided a better distribution of the reconstructed source, even better than the SP_3 based method. Second, using DE may deteriorate the quality of the reconstructed images. The more DE was used, especially in the lower wavelengths, the worse the quality of reconstructed images would be. This also proved the previously described problem concerning the difficulty in determining in which spectral band can the lower or higher order equation be used. To quantitatively evaluate these images, we calculated the

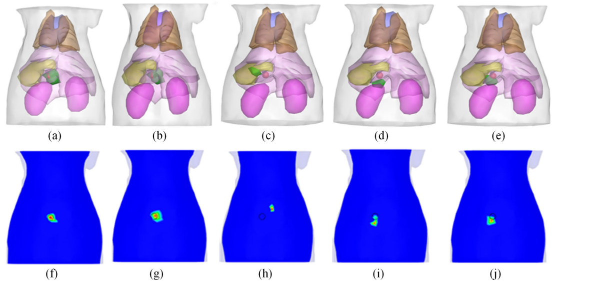

FIGURE 2. Reconstructed results obtained by the proposed and reference methods. (a)-(e) 3D views of the reconstructed results obtained by the AHSD, SP_3, DE, HSSD, and HSDD based methods respectively; (f)-(j) The corresponding XZ sectional images.

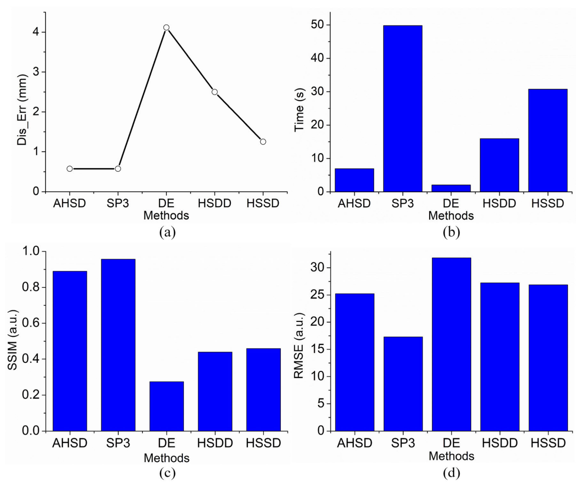

FIGURE 3. Quantitative evaluation of the AHSD based method and other reference methods. (a) the indicator of Dis_Err; (b) the indicator of Time; (c) the indicator of SSIM; (d) the indicator of RMSE.

indicators of Dis_Err, Time, SSIM and RMSE, as shown in Fig. 3, where Fig. 3(a) is the indicator of Dis_Err obtained by the proposed and reference methods, Fig. 3(b) plots the indicator of Time and Fig. 3(c) and Fig. 3(d) draw the indicators of SSIM and RMSE, respectively. Once more, almost the same conclusion can be made from these quantitative indicators. The AHSD and SP_3 based methods had the same Dis_Err value, which was much smaller than the other three methods. This is because SP_3, as a higher order approximation, has a higher accuracy than DE. The more the SP_3 was used, the smaller the Dis_Err value would be. Comparing the three hybrid models, AHSD had the best accuracy, HSSD came in second place and HSDD was the worst. This is because a single equation is used for the specific spectrum in the HSSD and HSDD models, and SP_3 is more used in HSSD than in HSDD. The same conclusions can be addressed from the other two evaluation factors of SSIM (Fig. 3(c)) and RMSE (Fig. 3(d)). In the quantitative evaluation of shape and distribution recovery, the result of the SP_3 based method was the best and the result of AHSD was very close to that of SP_3, followed by HSSD, HSDD and DE based ones.

Moreover, from the perspective of the Time indicator, the DE based method took the least time, and the AHSD based method took less time than the other three reference methods.

TABLE 2. Optical parameters at different wavelengths of different tissues in the real mouse based in vivo experiment [33]. In units of mm^{-1}.

Tissues	670 nm		620 nm		570 nm	
	μ_a	μ_s'	μ_a	μ_s'	μ_a	μ_s'
Muscle	0.086201	0.429071	0.202441	0.533968	1.685508	0.676851
Heart	0.058270	0.963871	0.137185	1.076926	1.203176	1.214520
Left Kidney	0.065341	2.253010	0.153714	2.532938	1.347580	2.875842
Right Kidney	0.065341	2.253010	0.153714	2.532938	1.347580	2.875842
Lung	0.194691	2.173884	0.456105	2.265106	3.614096	2.368331
Liver	0.348867	0.678066	0.822477	0.735596	7.218845	0.803493

This is because DE, as a lower order approximation, runs faster than the higher order SP_3. The more DE was used in the hybrid model, the less time it would take. Time was recorded on a personal computer with 3.2 GHz Intel(R) Core (TM) i5-6500 CPU and 8.00 GB RAM. The simulation results collectively demonstrated that our proposed AHSD based method is indeed an optimal option for multispectral CLT providing satisfactory accuracy with promising efficiency.

B. IN VIVO EXPERIMENT

The application potential of the proposed AHSD based method was then demonstrated with a living mouse based *in vivo* experiment. In this experiment, an athymic male nude mouse, approximately five to six weeks old, was used as the imaging mouse model. All procedures were performed in accordance with the guidance of the Air Force Military Medical University animal protocol. An artificial radioactive source was implanted into the liver of the living mouse to be used as the Cerenkov luminescent source. The artificial source was made of a glass vessel filled with approximately 400 μCi ^{18}F-FDG and had a diameter of 1 mm and a length of 5 mm. After gas anesthesia, the mouse was put into the imaging chamber of the small animal imaging system (IVIS Kinetic, PerkinElmer) for multispectral imaging. The CL images at the wavelengths of 570 nm, 620 nm and 670 nm were collected and used for the reconstruction. The micro-computed tomography (μCT) scans were performed using our homemade μCT system after the CL images were collected. The μCT system is composed of an X-ray tube (Oxford Instruments, Series 5000) and a flat panel detector (Hamamatsu, C7921CA-02). It should be noted that no contrast agent was injected during the μCT scan, making it difficult to clearly see the internal anatomy. Thus, the μCT images were registered onto a multi-atlas to obtain the anatomical structure on which heterogeneous reconstruction can be performed [44]. Fig. 1(b) shows the anatomical structure and related reference coordinate system. The obtained organs and the relevant optical parameters at the selected wavelengths are listed in Table 2. Similarly, the optical properties were calculated using the formula that is summarized in [43].

Before performing the reconstruction, the collected multispectral CL images were first mapped onto the surface of the mouse [45]. Fig. 4 presents the reconstructed results obtained by the proposed method in Fig. 4(a) and the other four reference methods in Fig. 4(b)-4(e). The central position of the implanted source can be retrieved from the reconstructed μCT images at the coordinate position of (51, 42, 33.5) mm. This *in vivo* experiment leads to a similar conclusion as the previous simulation. The AHSD based method has well recovered the position and distribution of the artificial radioactive source, with almost the same quality as that obtained by the SP_3 based method. Both of them have appropriately found the center of the artificial radioactive source. On the other hand, the HSSD and HSDD methods came second regarding performance, and finally came the DE based method. These insights can also be seen from the perspective of the Dis_Err indicator, as shown in Fig. 5. Similar to the above simulation results, since SP_3 has a better accuracy than DE, the more wavelengths the SP_3 was used in the reference methods, the better performance or the smaller Dis_Err could be obtained. Because the AHSD equation uses the hybrid model both in a specific spectral band and between different spectral bands, the accuracy of AHSD based method is better than that of HSSD and HSDD models. Taken together, these results confirmed the applicability of the AHSD based method for multispectral CLT of *in vivo* animal imaging.

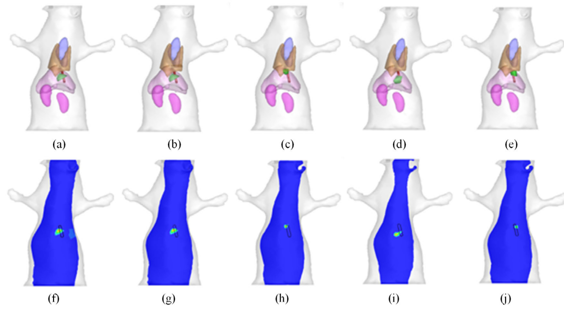

FIGURE 4. Reconstructed results obtained by the proposed and the reference methods. (a)-(e) 3D views of the reconstructed results obtained by the AHSD, SP3, DE, HSSD, and HSDD based methods, respectively; (f)-(j) Corresponding sectional images.

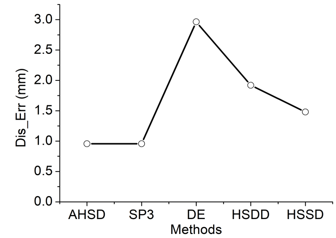

FIGURE 5. The values of the Dis_Err indicator obtained by the AHSD based method and the other reference methods.

IV. DISCUSSION AND CONCLUSION

In this work, we presented an adaptively hybrid 3rd simplified spherical harmonics with a reconstruction method based on the diffusion (AHSD) equation for multispectral CLT (mCLT), which fully considered and well utilized the wide spectrum characteristics of the CL signal. We showed that when applied to different spectra and different tissues at a certain spectrum, the AHSD based method provides better performance and wider applicability than the existing methods based on a single or hybrid equation. The performance and advantage of the AHSD based reconstruction method for multispectral CLT were evaluated using the digital mouse based simulation and artificial radioactive source based *in vivo* experiment. By combining advanced spectral unmixing methods [46], [47], that can effectively obtain multispectral CL images, we believe that the AHSD based reconstruction method will be suitable for multispectral CLT and will further promote various preclinical applications of CLT. In addition, Eq. (7) can be replaced by some advanced reconstruction models to obtain better results. Prospective studies will further focus on the biomedical applications of the AHSD based method.

REFERENCES

[1] H. Liu, G. Ren, S. Liu, X. Zhang, L. Chen, P. Han, and Z. Cheng, "Optical imaging of reporter gene expression using a positron-emission-tomography probe," *Proc. SPIE*, vol. 15, no. 6, 2010, Art. no. 060505.
[2] A. Ruggiero, J. P. Holland, J. S. Lewis, and J. Grimm, "Cerenkov luminescence imaging of medical isotopes," *J. Nucl. Med.*, vol. 51, no. 7, pp. 1123–1130, 2010.
[3] F. Boschi, L. Calderan, D. D'Ambrosio, M. Marengo, A. Fenzi, R. Calandrino, A. Sbarbati, and A. E. Spinelli, "*In vivo* ^{18}F-FDG tumour uptake measurements in small animals using Cerenkov radiation," *Eur. J. Nucl. Med. Mol. Imag.*, vol. 38, no. 1, pp. 120–127, 2011.
[4] K. Tanha, A. M. Pashazadeh, and B. W. Pogue, "Review of biomedical Čerenkov luminescence imaging applications," *Biomed. Opt. Express*, vol. 6, no. 8, pp. 3053–3065, 2015.
[5] X. Cao, Y. H. Zhan, X. Cao, J. M. Liang, and X. L. Chen, "Harnessing the power of Cerenkov luminescence imaging for gastroenterology: Cerenkov luminescence endoscopy," *Current Med. Imag. Rev.*, vol. 13, no. 1, pp. 50–57, 2017.
[6] T. M. Shaffer, E. C. Pratt, and J. Grimm, "Utilizing the power of Cerenkov light with nanotechnology," *Nature Nanotechnol.*, vol. 12, no. 2, pp. 106–117, 2017.
[7] P. A. Cerenkov, "Visible luminescence of pure liquids under action of γ-radiation," *Doklady Akademii Nauk*, vol. 2, no. 8, pp. 451–454, 1934.
[8] R. Robertson, M. S. Germanos, C. Li, G. S. Mitchell, S. R. Cherry, and M. D. Silva, "Optical imaging of Cerenkov light generation from positron-emitting radiotracers," *Phys. Med. Biol.*, vol. 54, no. 16, pp. N355–N365, 2009.
[9] S. B. Lee, G. Yoon, S.-W. Lee, S. Y. Jeong, B.-C. Ahn, D.-K. Lim, J. Lee, and Y. H. Jeon, "Combined positron emission tomography and Cerenkov luminescence imaging of sentinel lymph nodes using pegylated radionuclide-embedded gold nanoparticles," *Small*, vol. 12, no. 35, pp. 4894–4901, 2016.
[10] C.-C. Ke, Z.-M. He, Y.-J. Hsieh, C.-W. Huang, J.-J. Li, L. Hwu, Y.-A. Chen, B.-H. Yang, C.-W. Chang, W.-S. Huang, and R.-S. Liu, "Quantitative measurement of the thyroid uptake function of mouse by Cerenkov luminescence imaging," *Sci. Rep.*, vol. 7, no. 1, 2017, Art. no. 5717.
[11] S. Das, K. Haedicke, and J. Grimm, "Cerenkov-activated sticky tag for *in vivo* fluorescence imaging," *J. Nucl. Med.*, vol. 59, no. 1, pp. 58–65, 2018.
[12] S. Y. Jeong, M.-H. Hwang, J. E. Kim, S. Kang, J. C. Park, J. Yoo, J.-H. Ha, S.-W. Lee, B.-C. Ahn, and J. Lee, "Combined Cerenkov luminescence and nuclear imaging of radioiodine in the thyroid gland and thyroid cancer cells expressing sodium iodide symporter: Initial feasibility study," *Endocrine J.*, vol. 58, no. 7, pp. 575–583, May 2011.
[13] J. P. Holland, G. Normand, A. Ruggiero, J. S. Lewis, and J. Grimm, "Intraoperative imaging of positron emission tomographic radiotracers using Cerenkov luminescence emissions," *Mol. Imag.*, vol. 10, no. 3, pp. 177–186, 2011.
[14] H. Liu, C. M. Carpenter, H. Jiang, G. Pratx, C. Sun, M. P. Buchin, S. S. Gambhir, L. Xing, and Z. Cheng, "Intraoperative imaging of tumors using Cerenkov luminescence endoscopy: A feasibility experimental study," *J. Nucl. Med.*, vol. 53, no. 10, pp. 1579–1584, 2012.
[15] D. L. J. Thorek, D. S. Abou, B. J. Beattie, R. M. Bartlett, R. Huang, P. B. Zanzonico, and J. Grimm, "Positron lymphography: Multimodal, high-resolution, dynamic mapping and resection of lymph nodes after intradermal injection of ^{18}F-FDG," *J. Nucl. Med.*, vol. 53, no. 9, pp. 1438–1445, 2012.
[16] A. E. Spinelli, M. Ferdeghini, C. Cavedon, E. Zivelonghi, R. Calandrino, A. Fenzi, A. Sbarbati, and F. Boschi, "First human cerenkography," *Proc. SPIE*, vol. 18, no. 2, 2013, Art. no. 020502.
[17] D. L. J. Thorek, C. C. Riedl, and J. Grimm, "Clinical Cerenkov luminescence imaging of ^{18}F-FDG," *J. Nucl. Med.*, vol. 55, no. 1, pp. 95–98, 2014.
[18] H. Hu, X. Cao, F. Kang, M. Wang, Y. Lin, M. Liu, S. Li, L. Yao, J. Liang, J. Liang, Y. Nie, X. Chen, J. Wang, and K. Wu, "Feasibility study of novel endoscopic Cerenkov luminescence imaging system in detecting and quantifying gastrointestinal disease: First human results," *Eur. Radiol.*, vol. 25, no. 6, pp. 1814–1822, Jun. 2015.
[19] M. R. Grootendorst *et al.*, "Intraoperative assessment of tumor resection margins in breast-conserving surgery using ^{18}F-FDG Cerenkov luminescence imaging: A first-in-human feasibility study," *J. Nucl. Med.*, vol. 58, no. 6, pp. 891–898, 2017.
[20] C. Li, G. S. Mitchell, and S. R. Cherry, "Cerenkov luminescence tomography for small-animal imaging," *Opt. Lett.*, vol. 35, no. 7, pp. 1109–1111, 2010.
[21] Z. Hu, J. Liang, W. Yang, W. Fan, C. Li, X. Ma, X. Chen, X. Ma, X. Li, X. Qu, J. Wang, F. Cao, and J. Tian, "Experimental Cerenkov luminescence tomography of the mouse model with SPECT imaging validation," *Opt. Express*, vol. 18, no. 24, pp. 24441–24450, 2010.
[22] J. Zhong, J. Tian, X. Yang, and C. Qin, "Whole-body Cerenkov luminescence tomography with the Finite element SP_3 method," *Ann. Biomed. Eng.*, vol. 39, no. 6, pp. 1728–1735, 2011.
[23] C. Qin, J. Zhong, Z. Hu, X. Yang, and J. Tian, "Recent advances in Cerenkov luminescence and tomography imaging," *IEEE J. Sel. Topics Quantum Electron.*, vol. 18, no. 3, pp. 1084–1093, Jun. 2012.
[24] X. Ding, K. Wang, B. Jie, Y. Luo, Z. Hu, and J. Tian, "Probability method for Cerenkov luminescence tomography based on conformance error minimization," *Biomed. Opt. Express*, vol. 5, no. 7, pp. 2091–2112, 2014.
[25] J. Zhong, C. Qin, X. Yang, Z. Chen, X. Yang, and J. Tian, "Fast-specific tomography imaging via Cerenkov emission," *Mol. Imag. Biol.*, vol. 14, no. 3, pp. 286–292, 2012.
[26] Z. Hu, X. Chen, J. Liang, X. Qu, D. Chen, W. Yang, J. Wang, F. Cao, and J. Tian, "Single photon emission computed tomography-guided Cerenkov luminescence tomography," *J. Appl. Phys.*, vol. 112, no. 2, 2012, Art. no. 024703.
[27] J. Feng, K. Jia, G. Yan, S. Zhu, C. Qin, Y. Lv, and J. Tian, "An optimal permissible source region strategy for multispectral bioluminescence tomography," *Opt. Express*, vol. 16, no. 20, pp. 15640–15654, Sep. 2008.
[28] D. Yang, C. Yan, L. Yang, D. Peng, and X. Chen, "An alternative reconstruction framework with optimal permission source region for bioluminescence tomography," *Opt. Commun.*, vol. 427, pp. 112–122, Nov. 2018.
[29] A. E. Spinelli, C. Kuo, B. W. Rice, R. Calandrino, P. Marzola, A. Sbarbati, and F. Boschi, "Multispectral Cerenkov luminescence tomography for small animal optical imaging," *Opt. Express*, vol. 19, no. 13, pp. 12605–12618, 2011.
[30] H. Guo, X. He, M. Liu, Z. Zhang, Z. Hu, and J. Tian, "Weight multispectral reconstruction strategy for enhanced reconstruction accuracy and stability with Cerenkov luminescence tomography," *IEEE Trans. Med. Imag.*, vol. 36, no. 6, pp. 1337–1346, Jun. 2017.
[31] H. Liu, X. Yang, T. Song, C. Bao, L. Shi, Z. Hu, K. Wang, and J. Tian, "Multispectral hybrid Cerenkov luminescence tomography based on the finite element SP_n method," *Proc. SPIE*, vol. 20, no. 8, 2015, Art. no. 086007.
[32] X. Chen, F. Sun, D. Yang, S. Ren, Q. Zhang, and J. Liang, "Hybrid simplified spherical harmonics with diffusion equation for light propagation in tissues," *Phys. Med. Biol.*, vol. 60, no. 16, pp. 6305–6322, 2015.
[33] X. Chen, F. Sun, D. Yang, and J. Liang, "Coupled third-order simplified spherical harmonics and diffusion equation–based fluorescence tomographic imaging of liver cancer," *Proc. SPIE*, vol. 20, no. 9, 2015, Art. no. 090502.
[34] X. Chen, D. Yang, F. Sun, X. Cao, and J. Liang, "Adaptively alternative light-transport-model-based three-dimensional optical imaging for longitudinal and quantitative monitoring of gastric cancer in live animal," *IEEE Trans. Biomed. Eng.*, vol. 63, no. 10, pp. 2095–2107, Oct. 2016.

[35] H. Dehghani, D. T. Delpy, and S. R. Arridge, "Photon migration in non-scattering tissue and the effects on image reconstruction," *Phys. Med. Biol.*, vol. 44, no. 12, pp. 2897–2906, 1999.

[36] T. Tarvainen, M. Vauhkonen, V. Kolehmainen, S. R. Arridge, and J. P. Kaipio, "Coupled radiative transfer equation and diffusion approximation model for photon migration in turbid medium with low-scattering and non-scattering regions," *Phys. Med. Biol.*, vol. 50, no. 20, pp. 4913–4930, 2005.

[37] A. D. Klose and E. W. Larsen, "Light transport in biological tissue based on the simplified spherical harmonics equations," *J. Comput. Phys.*, vol. 220, no. 1, pp. 441–470, 2006.

[38] D. Yang, X. Chen, X. Cao, J. Wang, J. Liang, and J. Tian, "Performance investigation of SP_3 and diffusion approximation for three-dimensional whole-body optical imaging of small animals," *Med. Biol. Eng. Comput.*, vol. 53, no. 9, pp. 805–814, 2015.

[39] J. Feng, C. Qin, K. Jia, D. Han, K. Liu, S. Zhu, X. Yang, and J. Tian, "An adaptive regularization parameter choice strategy for multispectral bioluminescence tomography," *Med. Phys.*, vol. 38, no. 11, pp. 5933–5944, 2011.

[40] Q. Zhang, H. Zhao, D. Chen, X. Qu, X. Chen, X. He, W. Li, Z. Hu, J. Liu, J. Liang, and J. Tian, "Source sparsity based primal-dual interior-point method for three-dimensional bioluminescence tomography," *Opt. Commun.*, vol. 284, no. 24, pp. 5871–5876, 2011.

[41] Z. Wang, A. C. Bovik, H. R. Sheikh, and E. P. Simoncelli, "Image quality assessment: From error visibility to structural similarity," *IEEE Trans. Image Process.*, vol. 13, no. 4, pp. 600–612, Apr. 2004.

[42] Z. Chen, X. Jin, L. Li, and G. Wang, "A limited-angle CT reconstruction method based on anisotropic TV minimization," *Phys. Med. Biol.*, vol. 58, no. 7, pp. 2119–2141, 2013.

[43] G. Alexandrakis, F. R. Rannou, and A. F. Chatziioannou, "Tomographic bioluminescence imaging by use of a combined optical-PET (OPET) system: A computer simulation feasibility study," *Phys. Med. Biol.*, vol. 50, pp. 4225–4241, Sep. 2005.

[44] S. Ren, H. Hu, G. Li, X. Cao, S. Zhu, X. Chen, and J. Liang, "Multi-atlas registration and adaptive hexahedral voxel discretization for fast bioluminescence tomography," *Biomed. Opt. Express*, vol. 7, no. 4, pp. 1549–1560, 2016.

[45] X. Chen, X. Gao, D. Chen, X. Ma, X. Zhao, M. Shen, X. Li, X. Qu, J. Liang, J. Ripoll, and J. Tian, "3D reconstruction of light flux distribution on arbitrary surfaces from 2D multi-photographic images," *Opt. Express*, vol. 18, pp. 19876–19893, Sep. 2010.

[46] F. Luo, B. Du, L. Zhang, L. Zhang, and D. Tao, "Feature learning using spatial-spectral hypergraph discriminant analysis for hyperspectral image," *IEEE Trans. Cybern.*, vol. 49, no. 7, pp. 2406–2419, Jul. 2019.

[47] L. Zhang, L. Zhang, B. Du, J. You, and D. Tao, "Hyperspectral image unsupervised classification by robust manifold matrix factorization," *Inf. Sci.*, vol. 485, pp. 154–169, Jun. 2019.

LIN WANG received the B.S. degree in electrical engineering and automation and the master's degree in pattern recognition and intelligent systems from Xidian University, Xi'an, China, in 2007. She is currently pursuing the Ph.D. degree in computer application technology with Northwest University, Xi'an, China. Her current research interest includes the development of systems and algorithms in Cerenkov luminescence tomography and fluorescence molecular tomography.

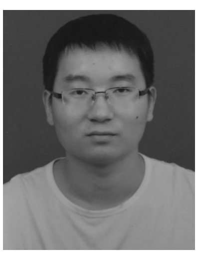

HONGHAO CAO received the B.S. degree in biotechnology from Xidian University, Xi'an, China, in 2017. He is currently pursuing the master's degree with the School of Life Science and Technology, Xidian University. His research interest includes the development of high-sensitive Cerenkov luminescence endoscope.

XIN CAO received the B.S. degree in electronic engineering and the Ph.D. degree in pattern recognition and intelligent systems from Xidian University, Xi'an, China, in 2011 and 2016, respectively.

Since 2016, he has been a Lecturer with the School of Information Science and Technology, Northwest University, Xi'an, China. His research interests include medical image analysis and optical molecular imaging.

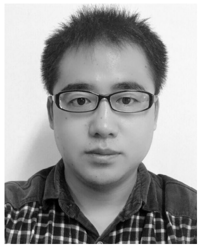

SHENGHAN REN received the B.S. degree in electronic engineering and the Ph.D. degree in pattern recognition and intelligent systems from Xidian University, Xian, China, in 2010 and 2017, respectively. Since 2017, he has been a Postdoctoral Researcher with the School of Life Science and Technology, Xidian University. His research interests include multimodality optical imaging, optical tomography, and deep learning methods for medical image processing.

KE LI received the Ph.D. degree in biomedicial engineering from Xi'an Jiaotong University, Xi'an, China, in 2016. From 2014 to 2016, he was a Visiting Scholar with the University of Kansas, USA. He is currently a Lecturer with the Institute of Basic and Translational Medicine, Xi'an Medical University. His research interests include multifunctional nanoparticles for diagnosis and the treatment of human diseases.

YONGHUA ZHAN received the Ph.D. degree in biomedical engineering from Xi'an Jiaotong University, Xi'an, China, in 2010. He is currently an Associate Professor with the School of Life Science and Technology, Xidian University, Xi'an, China. His research interest includes the development of molecular imaging probe and biomedical applications.

XUELI CHEN received the B.S. degree in biomedical engineering and the Ph.D. degree in pattern recognition and intelligent systems from Xidian University, in 2007 and 2012, respectively. From 2015 to 2017, he has been a Postdoctoral Researcher with Purdue University. He is currently a Professor with the School of Life Science and Technology, Xidian University. His research interests include multiscale, multimodality biophotonics imaging and its applications. He is currently a member of the OSA and SPIE.

XIAOWEI HE received the M.S. degree from the School of Electronic and Information Engineering, Xi'an Jiaotong University, Xi'an, China, in 2005, and the Ph.D. degree in pattern recognition and intelligent systems from the School of Life Sciences and Technology, Xidian University, Xi'an, in 2011.

Since 2016, he has been a Professor with the School of Information Sciences and Technology, Northwest University, Xi'an. His current research interests include medical imaging processing, 3D molecular imaging, and artificial intelligence.